

# ENSO surface shortwave radiation forcing over the tropical Pacific

K. G. Pavlakis<sup>1,2,3</sup>, N. Hatzianastassiou<sup>1,4</sup>, C. Matsoukas<sup>1,5</sup>, A. Fotiadis<sup>1,3</sup>, and I. Vardavas<sup>1,3</sup>

<sup>1</sup>Foundation for Research and Technology-Hellas, Heraklion, Crete, Greece

<sup>2</sup>Department of General Applied Science, Technological Educational Institute of Crete, Greece

<sup>3</sup>Department of Physics, University of Crete, Crete, Greece

<sup>4</sup>Laboratory of Meteorology, Department of Physics, University of Ioannina, Greece

<sup>5</sup>Department of Environment, University of the Aegean, Greece

Received: 12 February 2008 – Accepted: 4 March 2008 – Published: 7 April 2008

Correspondence to: K. Pavlakis (pavlakis@iesl.forth.gr)

Published by Copernicus Publications on behalf of the European Geosciences Union.

6697

## Abstract

We have studied the spatial and temporal variation of the downward shortwave radiation (DSR) at the surface of the Earth during ENSO events for a 21-year period over the tropical and subtropical Pacific Ocean (40° S–40° N, 90° E–75° W). The fluxes were computed using a deterministic model for atmospheric radiation transfer, along with satellite data from the ISCCP-D2 database, reanalysis data from NCEP/NCAR for the key atmospheric and surface input parameters, and aerosol parameters from GADS (acronyms explained in main text). A clear anti-correlation was found between the downward shortwave radiation anomaly (DSR-A) time-series, in the region 7° S–5° N 160° E–160° W located west of the Niño-3.4 region, and the Niño-3.4 index time-series. In this region where the highest in absolute value DSR anomalies are observed, the mean DSR anomaly values range from  $-45 \text{ Wm}^{-2}$  during El Niño episodes to  $+40 \text{ Wm}^{-2}$  during La Niña events. Within the Niño-3.4 region no significant DSR anomalies are observed during the cold ENSO phase in contrast to the warm ENSO phase. A high correlation was also found over the western Pacific (10° S–5° N, 120–140° E), where the mean DSR anomaly values range from  $+20 \text{ Wm}^{-2}$  to  $-20 \text{ Wm}^{-2}$  during El Niño and La Niña episodes, respectively. There is also convincing evidence that the time series of the mean downward shortwave radiation anomaly in the north subtropical Pacific region 7–15° N 150–170° E, precedes the Niño-3.4 index time-series by about 7 months. Thus, the downward shortwave radiation anomaly is a complementary index to the SST anomaly for the study of ENSO events and can be used to assess whether or not El Niño or La Niña conditions prevail.

## 1 Introduction

The El Niño Southern Oscillation (ENSO) is the dominant natural interannual climate fluctuation on Earth and involves the interaction between the tropical Pacific Ocean and the overlying atmosphere. However, its impact extends worldwide since heating of

6698

the tropical atmosphere creates changes in the global atmospheric circulation. Since Bjerknæs (1966, 1969) who first realized that the heart of the ENSO phenomenon is the ocean-atmosphere interaction, the dynamics of this pattern of climate variability, as well as variations in atmospheric and radiation variables associated with it, were studied by many workers (e.g., Philander, 1990; McCreary and Anderson, 1991; Neelin et al., 1998; Chou et al., 2004; Dijkstra, 2006; Wang and Fiedler, 2006; Pavlakis et al., 2007). Under normal conditions, the equatorial Pacific Ocean is characterized by warm surface waters in the west and cold surface waters in the east and by easterly trade winds in the lower atmosphere (Walker circulation). The trade winds as they flow over the Pacific Ocean pick up heat and moisture, bringing warm moist air over the Indonesian region (western Pacific) where it ascends and deep convection causes heavy precipitation. The warm phase of ENSO (El Niño) is associated with an unusual surface water warming of the eastern and central equatorial Pacific, a weakening of the easterly trade winds and a shift of strong convection from the western Pacific, where dry conditions prevail, into the central Pacific accompanied by heavier than usual rainfall there. La Niña, the ENSO cold phase, is the counterpart of El Niño, often following it and characterised by the opposite effects. Thus, ENSO is an oscillation between warm and cold events with a peak that typically occurs during the northern hemisphere winter (late December–early January). Over the past two decades a large number of studies have appeared, attempting to explain the mechanism of the oscillation between the two phases of the ENSO phenomenon and many models have been proposed (e.g. Suarez and Schopf, 1988; Cane et al., 1990; Jin, 1997a, 1997b; Picaut et al., 1997; Wang et al., 1999; Wang, 2001; Wang and Picaut, 2004). A more recent short review summarizing theories and mechanisms about El Niño variability is given by Dijkstra (2006).

Despite recent progress, the ENSO onset time, duration, strength and spatial structure have proved hard to simulate and forecast since it involves complex climatic processes and feedbacks between atmospheric and ocean properties (e.g. Fedorov et al., 2003, and references therein). Thus, measurements of different atmospheric and

6699

ocean properties are essential to improve our understanding of ENSO evolution. International monitoring programs of the coupled atmosphere-ocean system started in the Pacific around 1985 and led to the TAO/TRITON (Tropical Atmosphere Ocean project/Triangle Trans Ocean Buoy Network) array of moored buoys across the ocean. The aim of this program is to provide real-time ground-based measurements of winds, sea-surface temperature, sub-sea-surface temperature, sea level and ocean flow that help in the understanding of the physical processes responsible for ENSO (McPhaden et al., 1998). Satellite observations on the other hand, provide measurements of atmospheric variables that include precipitation, cloud cover, humidity, and the radiation budget at the top of the atmosphere (Trenberth and Caron, 2000; Cess et al., 2001; Allan et al., 2002; Wagner et al., 2005; Wang and Fiedler, 2006). The variability and the spatial distribution of the values of ocean and atmospheric variables are not the same for all ENSO events. Thus, a definition of ENSO is necessary for the study of this phenomenon (Trenberth, 1997) using some of the ocean or atmospheric parameters for constructing an index to describe the phase and strength of ENSO events. Several different indices have been used in the literature, mostly based on SST. The SST based indices are obtained from the SST anomalies with respect to average values, over some specified region of the ocean (see for example, Trenberth and Stepaniak, 2001; Hanley et al., 2003). There is another index widely used, the Southern Oscillation index, which is related to air pressure differences at sea level, between Darwin (Australia) in the west and Tahiti in the east. There has been also an effort to combine several atmospheric-oceanic variables into a single index like the multivariate ENSO index (Wolter and Timlin, 1998). Averages of 850 mb wind, outgoing longwave radiation (OLR) at the top of the atmosphere as well as precipitation over specific regions (Curtis and Adler, 2000) are also used, although not often, to monitor ENSO. Recently (Pavlakis et al., 2007) presented the downwelling longwave radiation (DLR) anomaly in the Niño-3.4 region as a useful index that contains information both for oceanic (i.e. SST) and atmospheric (i.e. water vapour, cloud amount) processes.

6700

Although satellites monitor the Earth's radiation budget at the top of the atmosphere, they do not measure radiative fluxes at the Earth's surface. However, the Earth's climate system is driven by the radiative energy balance between the solar shortwave radiation (SW) absorbed by the atmosphere and the surface of the Earth and the thermal longwave radiation (LW) emitted by the Earth to space. In this respect, ENSO events are expected to be associated with the spatial and temporal variability of the radiative energy balance at the surface over the tropical and subtropical Pacific ocean. Therefore, radiative transfer models remain as the only alternative for estimating the surface radiation budget variability and its influence on ENSO evolution. Specifically, the net heat flux into the ocean plays a key role in ENSO evolution and it is a significant variable in the models that have been developed to make ENSO predictions (Dijkstra, 2006). The variation of the net heat flux during ENSO events is of paramount importance to the dynamics of the system (Harrison et al., 2002; Chou et al., 2004). The net heat flux into the ocean is a small residual of four terms; the net shortwave radiation at the surface (NSR), the latent heat loss, the sensible heat transfer and the net downwelling longwave radiation at the Earth's surface (NSL). The NSL is the difference between the downward longwave radiation (DLR) at the Earth's surface and the Earth's surface thermal emission. In a previous paper (Pavlakis et al., 2007) we presented the NSL and DLR as well as their variability over the tropical and subtropical Pacific ocean during the warm and cold ENSO phases. There, the DLR-A [3.4] index based on DLR anomalies in the Niño 3.4 region was defined as a useful index to describe ENSO events and the DLR anomalies were used as a useful variable reflecting SST changes and water vapour variability in the lower atmosphere (see also Vardavas and Taylor, 2007). The NSR is the difference between the downwelling shortwave radiation (DSR) and the reflected radiation from the ocean surface. However, the reflected term is more than one order of magnitude smaller than the DSR, since the ocean albedo is less than 0.07. Thus, DSR dominates the net shortwave flux budget. The variability of DSR, the component of the net heat into the ocean with the largest magnitude, reflects mostly fluctuations in cloud cover caused by variations in atmospheric circulation and thus,

6701

it is very important in order to describe and study the intensity or duration of ENSO events.

Thus in this paper, we present DSR data generated by a deterministic radiation transfer model for the period 1984–2004 for the tropical and subtropical Pacific Ocean and examine their spatial and temporal variability during ENSO events. In addition, we investigate the correlation of DSR anomalies with the Niño 3.4 index. In Sect. 2, we describe the radiation model and the input data used. In Sect. 3, the surface shortwave radiation distribution and its variation during warm and cold mature ENSO phases are presented. In Sect. 4, the DSR variation during ENSO evolution is examined. In Sect. 5, the correlation of the Niño 3.4 index and surface radiation parameters are presented. In Sect. 6, we present our conclusions. Table 1 lists the symbol definitions of the radiation parameters that are most often used in this paper.

## 2 Radiation model and data description

We use a shortwave (SW) radiative transfer model which is described in detail in Hatzianastassiou et al. (2004a) and Hatzianastassiou et al. (2005), where it was used to compute the top of the atmosphere (TOA) and surface SW radiation-budgets on a global scale. This model is based on a detailed radiative-convective model developed for climate change studies (Vardavas and Carver, 1984; Vardavas and Taylor, 2007) and has been successfully tested (Hatzianastassiou and Vardavas, 1999, 2001) according to the Intercomparison of Radiation Codes in Climate Models (ICRCCM) program. The model results have been validated against Earth Radiation Budget Experiment (ERBE) S4 scanner data (Hatzianastassiou et al., 2004a) as well as against data from the Baseline Surface Radiative Network (BSRN) (Ohmura et al., 1998) and the Global Energy Balance Archive (GEBA) (Ohmura and Gilgen, 1993) in Hatzianastassiou et al. (2005). The same model has been also used on a regional scale to study trends in tropical mean SW radiation budget at TOA (Fotiadi et al., 2005) as well as to compute the spatial and temporal distribution of long-term shortwave surface radiation

6702

over Greece (Fotiadi et al., 2006).

In brief, the model divides the SW radiation into two spectral bands, one essentially for the ultraviolet-visible wavelengths ( $\lambda < 0.85 \mu\text{m}$ ), accounting for about 60% of the total solar radiation, and a second band for the near-infrared wavelengths (5  $0.85 \mu\text{m} \leq \lambda \leq 5 \mu\text{m}$ ) accounting for about 40% of total solar radiation. The model takes into account the presence of ozone ( $\text{O}_3$ ), water vapor ( $\text{H}_2\text{O}$ ), carbon dioxide ( $\text{CO}_2$ ), aerosol particles and Rayleigh scattering layers as well as low-, middle- and high-level cloud layers in the atmosphere, all above an isotropically reflecting Earth surface. The atmosphere is divided vertically in layers of about 5 hPa thickness and surface topog- 10 raphy is considered. The surface reflectivity is computed for every pixel by considering four types of surface: land, ocean, snow and ice. A full presentation and discussion of the model can be found in Hatzianastassiou et al. (2005).

All of the cloud climatological data for our radiation transfer model were taken from the International Satellite Cloud Climatology Project (ISCCP-D2) data set (Rossow and Schiffer, 1999), the latest released ISCCP series of mean monthly cloud clima- 15 tologies, which provides monthly means for 72 climatological variables in 2.5-degree equal-angle grid-boxes for the period 1984–2004. The specific variables used in our model from ISCCP-D2 database are summarized in Fotiadi et al. (2006). The vertical profiles of the temperature and water vapour as well as the surface temperature were taken from the National Center for Environmental Prediction / National Centers for Atmospheric Research (NCEP/NCAR) reanalysis project (Kistler et al., 2001), corrected for topography as in Hatzianastassiou et al. (2001). These data are also on a 20 2.5-degree spatial resolution, monthly averaged and cover the same 21-year period as the ISCCP-D2 data. Data for aerosol optical depth, single scattering albedo and asymmetry parameter were taken from GADS (Koepke et al., 1997). A complete description of the aerosol data used is given in Hatzianastassiou et al. (2004b), and the treatment of aerosols in the SW model is described in Hatzianastassiou et al. (2005).

A full presentation and discussion of the DSR distribution over the globe can be found in Hatzianastassiou et al. (2005). There, a series of sensitivity tests were performed

6703

to investigate how much uncertainty is introduced in the model DSR by uncertainties in the input parameters, such as low, middle or high cloud amount, cloud absorption and scattering optical depth, cloud asymmetry factor as well as the total precipitable water. Also, comparisons between the monthly mean DSR fluxes used in this paper 5 and those of higher spatial ( $1^\circ \times 1^\circ$  latitude-longitude) or temporal (daily) resolution, both on a global and regional scale, have shown very good agreement, with correlation coefficients exceeding 0.98 (see Hatzianastassiou et al., 2005; Fotiadi et al., 2006).

### 3 Long-term surface shortwave radiation

The geographical distribution of the downward SW radiation (DSR) at the Earth's surface for each month of the 21-year period 1984–2004 was computed at a spatial resolu- 10 tion of  $2.5^\circ(\text{latitude}) \times 2.5^\circ(\text{longitude})$ , over the tropical and subtropical Pacific Ocean ( $40^\circ \text{S} - 40^\circ \text{N}$ ,  $90^\circ \text{E} - 75^\circ \text{W}$ ). During the 21-year study period (1984–2004) five significant El Niño events occurred (1986–1987, 1991–1992, 1994–1995, 1997–1998 and 2002–2003) and the same number of significant La Niña events in 1984–1985, 1988– 15 1989, 1998–1999, 1999–2000 and 2000–2001 (Trenberth, 1997; Wang and Fiedler, 2006).

We have calculated, for each  $2.5 \times 2.5$  grid-box, the mean monthly DSR averaged over the 11 neutral years ( $\text{DSR}_{\text{NE}}$ ), i.e., the years when no significant El Niño or La Niña events occurred, as a representative of normal conditions. The  $\text{DSR}_{\text{NE}}$  for the 3- 20 month period November, December and January (NDJ) is shown in Fig. 1a (top panel). The three month period NDJ is selected as best representing the mature phase of ENSO evolution, as the ENSO peak typically occurs during December–January when the strongest changes in the DSR occur.

As expected, the maxima in DSR over the ocean, reaching about  $280 \text{ Wm}^{-2}$ , occur 25 over the eastern Pacific (east of the date line), in the region near the equator ( $5^\circ \text{S} - 5^\circ \text{N}$ ) and in the southeastern subtropics ( $5^\circ \text{S} - 30^\circ \text{S}$   $140^\circ \text{W} - 100^\circ \text{W}$ ), where subsidence regions are located with small total cloud amounts (Tian and Ramanathan, 2002). Over

6704

the eastern Pacific, low values of DSR, about  $170 \text{ Wm}^{-2}$ , are observed along the coasts of Peru and west of the peninsula of Baja California where low-level clouds are predominant (Tian and Ramanathan, 2002; Amador et al., 2006) while even lower values of DSR of about  $150 \text{ Wm}^{-2}$  are found in the inter-tropical convergence zone (ITCZ) centered around  $8^\circ \text{ N}$ , a region of strong upward motion of moist air.

Over the west tropical Pacific (west of the date line), there is a single Hadley cell with the air rising over the western Pacific warm pool ( $10^\circ \text{ S}$ – $10^\circ \text{ N}$ ) where the highest open ocean water temperatures on Earth are observed. Thus high level clouds (cloud amount over 40%) are concentrated in these moist convective regions (Tian and Ramanathan, 2002) and low DSR values of about  $190$ – $220 \text{ Wm}^{-2}$  are observed there. Note that there is a difference of about  $60$ – $70 \text{ Wm}^{-2}$  in DSR values between eastern and western Pacific around the equator.

We also computed, for each grid-box, the average DSR over the five years<sup>1</sup> when El Niño ( $\text{DSR}_{\text{EN}}$ ) conditions prevailed (Fig. 1b, middle panel) and the corresponding average DSR over the five years when La Niña ( $\text{DSR}_{\text{LN}}$ ) conditions prevailed (Fig. 1c, bottom panel), for the three month period of NDJ. It is evident from these figures that lower values of DSR are observed over the central and eastern Pacific, during the El Niño years due to the shift of atmospheric convection from the western Pacific warm pool to the central equatorial Pacific. Thus the east-west Pacific DSR gradient becomes smaller. On the other hand, high DSR values of up to  $270 \text{ Wm}^{-2}$  are observed west of the date line during the La Niña years (Fig. 1c).

In Fig. 2 we show the distribution of the difference  $\text{DSR}_{\text{EN}} - \text{DSR}_{\text{LN}}$ , over the tropical and subtropical Pacific. This difference will be referred to as the El Niño DSR anomaly ( $\text{DSR-A}_{\text{LN}}$ ) with respect to La Niña DSR. In the same figure, the rectangle designates the Niño-3.4 region ( $5^\circ \text{ S}$ – $5^\circ \text{ N}$ ,  $170$ – $120^\circ \text{ W}$ ) that is used to define the Niño-3.4 index, one of the indices based on sea surface temperature, for monitoring and identifying El Niño and La Niña events (Hanley et al., 2003). The Niño-3.4 region is used widely

<sup>1</sup>An “El Niño year” is defined, for our purposes, as starting in July and ending in June of the next year.

6705

as a region with high SST anomalies and with a proximity to the main deep-convection centres during ENSO events. As can be seen in Fig. 2 the  $\text{DSR-A}_{\text{LN}}$  obtains the highest values (in absolute terms), reaching a maximum of about  $-80 \text{ Wm}^{-2}$ , near the equator west of the Niño-3.4 region where the largest anomalies in sea surface temperatures (SST) are observed during El Niño events. Inside the Niño-3.4 region as well as in a region near the coast of Peru ( $0$ – $5^\circ \text{ S}$ ,  $120$ – $90^\circ \text{ W}$ )  $\text{DSR-A}_{\text{LN}}$  is about  $-30 \text{ Wm}^{-2}$ . In the western Pacific, on the other hand, the sign of the  $\text{DSR-A}_{\text{LN}}$  is reversed, with the  $\text{DSR}_{\text{EN}}$  being higher than  $\text{DSR}_{\text{LN}}$  by  $+30 \text{ Wm}^{-2}$  east of Borneo, north of Australia and over the Philippines Sea.

#### 4 DSR variation during ENSO evolution

Here we investigate the evolution of ENSO-related changes in the distribution and values of DSR over the tropical and subtropical Pacific. In our subsequent analysis we use the three month period of August, September and October (ASO) to study the early stages of ENSO development, November, December and January (NDJ) for the mature phase of El Niño or La Niña events, and February, March and April (FMA) for the decay phase of ENSO as in Pavlakis et al. (2007). In spite of the significant differences in the onset and evolution of individual ENSO events, the ASO, NDJ, and FMA periods provide a frame of reference for studying, in broad terms, the evolution of ENSO.

##### 4.1 El Niño events

We now define the difference  $\text{DSR}_{\text{EN}} - \text{DSR}_{\text{NE}}$  as the El Niño DSR anomaly with respect to the average normal condition (El Niño  $\text{DSR-A}_{\text{NE}}$ ). In Fig. 3 (left-hand side) we show the distribution of El Niño  $\text{DSR-A}_{\text{NE}}$  for the three-month periods of ASO (top panel), NDJ (middle panel) and FMA (bottom panel), at  $2.5 \times 2.5$  spatial resolution. In order to investigate and identify the regions that show significant changes in the DSR during El Niño years with respect to values under normal conditions, we performed for each

6706

grid-box and for each three-month period (ASO, NDJ, FMA) a two-tailed Student's t-test. Our two samples are the three-monthly DSR values of the 11 neutral years within our study period 1984–2004 and the corresponding values for the 5 years when El Niño conditions prevailed. The null hypothesis is that the mean values of the two samples are equal and the alternative hypothesis is that these values are different. On the right-hand side of Fig. 3 we show the geographical distribution of the P-values for the ASO (top panel), NDJ (middle panel) and FMA (bottom panel). Grid-boxes with P-values smaller than 0.05 are considered to have statistically significant El Niño DSR- $A_{NE}$  values.

The lowest values of DSR- $A_{NE}$  during the early stage of El Niño development (around  $-35 \text{ Wm}^{-2}$ ) are found in the equatorial Pacific west of the Niño-3.4 region, the area where high positive SST anomalies (ocean warming) are observed (Wang, 2002). In contrast, high DSR- $A_{NE}$  values around  $+25 \text{ Wm}^{-2}$  are observed in the equatorial western Pacific over Indonesia east of Borneo. It is the same region ( $5^\circ \text{ S} - 5^\circ \text{ N}$ ,  $120 - 140^\circ \text{ E}$ ), termed Niño-5 by Wang and Weisberg (2000), where westerly wind anomalies were found to peak about six to eight months before those in the Niño-4 region. Values of DSR- $A_{NE}$  around  $-20 \text{ Wm}^{-2}$  are observed over the region  $150 - 180^\circ \text{ E}$  centred near  $10^\circ \text{ N}$ , which is consistent with the intensification of ascending air motion in roughly the same region as shown by Wang (2002) during the ENSO transition phase (the three month period of July, August, and September prior to the El Niño peak). For all the regions referred to above the statistical significance of the anomalies is very high with P-values lower than 0.01.

During the mature phase of El Niño, negative values of DSR- $A_{NE}$  are observed in a region confined around the equator, between  $10^\circ \text{ S} - 5^\circ \text{ N}$  that extends from  $160^\circ \text{ E}$  to the coast of Peru. The lowest values of the DSR- $A_{NE}$  reach about  $-60 \text{ Wm}^{-2}$ , and are observed over the region where the deep atmospheric convection shifts from the western Pacific warm pool, west of the warmest SST anomalies in the Niño-3.4 and Niño-4 regions. The P-values there are the lowest observed over the whole Pacific (less than 0.001). There opaque clouds associated with deep convection, are bright

6707

reflectors of solar radiation and thus act to reduce the surface solar radiation. In the same region, negative outgoing longwave radiation (OLR) anomalies are observed at the top of the atmosphere (Wang, 2000; Wang and Fiedler, 2006) because due to deep convection, cloud tops get higher, and the radiation to space from clouds is at a lower temperature. No significant downward longwave radiation anomalies (DLR-As) are observed at the surface of the ocean (Pavlaklis et al., 2007) and thus, in this region, DSR is the radiative component that mostly contributes to the fluctuation of the net heat flux into the ocean during El Niño. The maximum DLR-As about  $20 \text{ Wm}^{-2}$ , are observed within the Niño-3.4 region causing radiative warming of the ocean surface there (Pavlaklis et al., 2007) and coincide with the high SST anomalies. The SST anomalies are linked to the water vapour content of the atmosphere whose fluctuation in the lower atmosphere is the major factor that causes the DLR-As. In the Niño-3.4 region the mean value of DSR- $A_{NE}$  is about  $-30 \text{ Wm}^{-2}$ , and thus the radiative cooling of the ocean surface, during the warm ENSO phase, is moderated with respect to the neighbouring west of Niño-3.4 tropical region. In the west Pacific DSR- $A_{NE}$  values are of opposite sign (positive), they are smaller in absolute magnitude than those in the eastern/central Pacific and are observed off the equator, north of Australia, north of New Guinea and over the Philippines and part of the South China Sea, with P-values less than 0.03.

During the decay phase of El Niño, DSR variability is centred along the equator in the central Pacific. Values of DSR- $A_{NE}$  around  $-30 \text{ Wm}^{-2}$  are observed roughly in the same equatorial central Pacific region as during the mature ENSO phase, but in the eastern Pacific this region now shifts north of the equator up to the south coast of Mexico ( $20^\circ \text{ N}$ ). The out-of-phase behaviour in DSR- $A_{NE}$  values between the eastern and the western Pacific is also observed during the decay phase of El Niño. In the western Pacific DSR- $A_{NE}$  values of up to  $+20 \text{ Wm}^{-2}$  with high statistical significance (P-values less than 0.02) are observed over the South China Sea, while the feature observed north of Australia during the mature ENSO phase has now migrated south-eastward.

6708

## 4.2 La Niña events

A similar analysis was conducted for the DSR anomalies during La Niña events. The various parameters are defined in the same way as in Sect. 4.1, but for the La Niña years. Instead of the suffix EN (El Niño), we use here the suffix LN (La Niña). The resulting geographical distribution of the La Niña DSR anomalies ( $DSR-A_{NE}$ ), with respect to normal conditions, is shown on the left in Fig. 4 in the top panel for ASO, the middle panel for NDJ and the bottom panel for FMA. Large positive values (i.e. higher DSR for the La Niña years) of about  $+40 \text{ Wm}^{-2}$  are observed west of the dateline, in the region  $7^\circ \text{ S} - 5^\circ \text{ N}$ ,  $160 - 180^\circ \text{ E}$  during the mature ENSO phase (i.e. during NDJ) while the corresponding values during the early phase of La Niña are about  $30 \text{ Wm}^{-2}$  over the same region. On the right side of Fig. 4 we present the geographical distribution of P-values, which confirms that the region west of the dateline, indicated above, displays statistically significant anomalies during all three phases (i.e. ASO, NDJ, FMA) of La Niña with P-values less than 0.02.

Note that there are no significant values of the  $DSR-A_{NE}$  in the Niño-3.4 region during the mature La Niña phase in contrast to the El Niño phase. In contrast, significant DLR-A with a mean value of about  $-15 \text{ Wm}^{-2}$  is observed in the same region during ENSO cold phase (Pavlakís et al., 2007) and thus, DLR is the radiative component that mainly contributes there to the fluctuation of the net heat flux into the ocean during the ENSO cold phase.  $DSR-A_{NE}$  values near  $-25 \text{ Wm}^{-2}$  are observed around the equator in the western Pacific east of Borneo and over Indonesia during the mature phase but the feature splits into two sub-features north and south of the original feature during the La Niña decay phase.

## 5 Correlation of Niño-3.4 index and DSR anomaly

The Niño-3.4 index based on sea surface temperature (SST) is used extensively in recent years for identifying El Niño or La Niña events. The strength of the events

6709

is quantified as the three-month smoothed SST departures from normal SST, in the Niño-3.4 region of the equatorial Pacific. In Fig. 5 we show the geographical distribution of the correlation coefficient given by linear regression of the time-series of the anomaly of the mean monthly DSR at the surface with respect to the average monthly DSR for the whole study period 1984–2004 ( $DSR-A$ ) in each  $2.5 \times 2.5^\circ$  grid-box and the Niño-3.4 index time-series. Although there are low values of the correlation coefficient (anti-correlation) over the entire Niño-3.4 region, the minimum values of the correlation coefficient (strongest anti-correlation) are observed west of the Niño-3.4 region in the zone  $7^\circ \text{ S} - 5^\circ \text{ N}$   $160^\circ \text{ E} - 160^\circ \text{ W}$ . This region will be referred to as the central Pacific region. The centre of deep convection is located there and the clouds that are formed block the downwelling solar radiation and at the same time (i.e. during the peak of the warm ENSO phase) the highest SSTs anomalies are observed in the Niño-3.4 region. In the western Pacific there is a positive correlation between the  $DSR-A$  and Niño-3.4 index time-series although in absolute terms the correlation coefficients are not as high as in the central Pacific. The maximum values of the correlation coefficient in the western Pacific are observed in the region  $10^\circ \text{ S} - 5^\circ \text{ N}$   $120 - 140^\circ \text{ E}$ , which will be referred to as the western Pacific region. Finally, another very interesting region is the  $7 - 15^\circ \text{ N}$   $150 - 170^\circ \text{ E}$  region (we shall refer to this as the north subtropical region), where although the correlation coefficients are very low there is a time shift between the  $DSR-A$  time series and the Niño-3.4 index time-series (we analyze these time-series later in this section).

We have calculated the 3-month smoothed anomaly of the mean monthly DSR at the surface with respect to the average monthly DSR for the whole study period 1984–2004 ( $DSR-A$ ), for each of the Niño-3.4, central Pacific, western Pacific and north subtropical region, respectively.

Figure 6a shows the time-series of the  $DSR-A$  for the period 1984–2004 (black line) for the Niño-3.4 region. For comparison we have overlaid on the same diagram the time-series of the Niño-3.4 SST index (red line). There is a clear anti-correlation between the two time-series. It is also evident that the maximum DSR change during

6710

warm (El Niño) or cold (La Niña) ENSO events occurs between November and January. The DSR-A during the 1991–1992 and 1997–1998 El Niños take the highest absolute values (about  $55 \text{ Wm}^{-2}$ ) because during these events the centre of convective activity has moved into the Niño-3.4 region. Note however that the absolute values of DSR-A during the warm ENSO events are much higher than the corresponding values during cold ENSO events. This is due to the fact that the region of significant DSR anomalies during the cold ENSO phase lies to the west of the Niño-3.4 region (see Fig. 4a and b and discussion there). Thus, by means of DSR-A, no signal is observed in the Niño-3.4 region during the La Niña phase as clearly shown in Fig. 7a where a scatter plot between DSR-A in Niño-3.4 region and the Niño-3.4 index is presented.

Figure 6b shows the time-series of the DSR-A (black line) in the central Pacific region ( $7^\circ \text{ S} - 5^\circ \text{ N } 160^\circ \text{ E} - 160^\circ \text{ W}$ ) and on the same diagram we have overlaid the time-series of the Niño-3.4 SST index (red line). The DSR-A is out-of-phase with the Niño-3.4 index. There is an excellent anti-correlation in two neighbouring regions between the Niño-3.4 index (a sea parameter) over the Niño-3.4 region and the DSR-A over the central Pacific region that reflects mostly the variations in cloud amount caused by atmospheric circulation anomalies. We have calculated the 3-month smoothed anomaly of the mean monthly total cloud amount with respect to the average monthly total cloud amount for the study period 1984–2004 for the central Pacific region. A linear regression between the DSR-A time series and the total cloud amount anomaly time series yielded a correlation coefficient of  $r = -0.91$  (anti-correlation) showing that cloud amount variations are the primary determinants of the DSR variability. Thus in the central Pacific region the high DSR-A is correlated but not collocated with the region of high anomalies in SST (Niño-3.4 region). The DSR-A in the central Pacific has values as low as  $-45 \text{ Wm}^{-2}$  (during the 1986–1987 El Niño), and as high as  $+40 \text{ Wm}^{-2}$  (during the 1999–2000 La Niña). Note that the 1991–1992 and 1997–1998 ENSO warm events are not the strongest ones with respect to the DSR anomaly. However, for all ENSO events (both warm and cold) high DSR-A values are observed, in absolute terms. A linear regression between DSR-A time-series in the central Pacific

6711

region and the Niño-3.4 index yielded a correlation coefficient of  $r = -0.83$  and a slope of  $-15.4 \pm 0.6 \text{ Wm}^{-2} / ^\circ\text{C}$ , as shown in Fig. 7b.

In the western Pacific region ( $10^\circ \text{ S} - 5^\circ \text{ N } 120 - 140^\circ \text{ E}$ ) there is a positive correlation between the time-series of DSR-A and the Niño-3.4 index, as shown in Fig. 8a. In both time-series there are clear peaks during El Niño events and minima for the La Niña events. The relative strengths of warm and cold ENSO events are very similar with DSR-A values reaching as high as  $+20 \text{ Wm}^{-2}$  during the 1991–1992, 1997–1998 and 2002–2003 El Niño events and as low as  $-20 \text{ Wm}^{-2}$  during the 1988–1989, 1995–1996 and 1998–1999 La Niña events. Linear regression between DSR-A time-series in the western Pacific region and the Niño-3.4 index yielded a correlation coefficient of  $r = 0.78$  and a slope of  $8.8 \pm 0.4 \text{ Wm}^{-2} / ^\circ\text{C}$ , as shown in Fig. 8b.

In the north subtropical Pacific region the 3-monthly smoothed DSR anomalies seem to precede the appearance of significant SST anomalies in the Niño-3.4 region (Niño-3.4 index) as shown in Fig. 9a. It is clear that the DSR-A shows a minimum before the peak of the Niño-3.4 index for each El Niño event. The minimum value of the DSR-A is about  $-20 \text{ Wm}^{-2}$  before the 1991–1992, 1997–98, and the 2002–2003 El Niño. We have, subsequently, calculated the correlation coefficient between the Niño-3.4 index time-series and the average 3-monthly smoothed DSR-A time-series in the north subtropical Pacific region shown in Fig. 9a, shifted by up to 12 months. In Fig. 9c we have plotted the value of this correlation coefficient (the values are negative, because the DSR anomalies and the Niño-3.4 index are anti-correlated) as a function of the time lag introduced in months. It is obvious that the highest anti-correlation is observed when the DSR-A time-series is shifted by 7 months. The value of the correlation coefficient decreases from  $-0.09$  with no time shift (no correlation), to  $-0.61$  with a 7-month time shift. This means that DSR anomalies in the north subtropical Pacific region precede the anomalies in the Niño-3.4 region by 7 months. In Fig. 9b where the DSR-A time-series has been shifted by 7 months are shown clear minima of DSR-A for each peak of the Niño-3.4 index. Wang (2002) also found an anomalous ascending motion near  $10\text{N}$  and  $120-170\text{E}$  during the El Niño transition phase, i.e. 5–6 months prior to

6712

each El Niño peak (note the overlap of our north subtropical Pacific region with that of Wang (2002)).

## 6 Conclusions

Our model calculations, which are based on ISCCP-D2 cloud climatologies, temperature and humidity profile information from NCEP/NCAR reanalysis and aerosol data from GADS, show a high variability in the downward shortwave radiation (DSR) at the surface of the Earth over the tropical and subtropical Pacific Ocean during ENSO events. We have found that the DSR decreases during warm ENSO phases, compared with neutral years, in a broad area in the central and eastern Pacific. This decrease in DSR ( $DSR-A_{NE}$ ), for the three-month period November, December and January, corresponding to the mature phase of El Niño is larger than  $15 \text{ Wm}^{-2}$ , in a broad area around the equator in the central Pacific extending to the coast of South America. A minimum  $DSR-A_{NE}$  of about  $-60 \text{ Wm}^{-2}$ , is observed west of the Niño-3.4 region. The DSR variability is associated mainly with variations in cloud amount. An increase in the amount of opaque and hence more reflecting clouds associated with deep convection results in less solar radiation reaching the surface.

During the cold phases of ENSO in the central Pacific, values of  $DSR-A_{NE}$  greater than  $+30 \text{ Wm}^{-2}$  are observed west of the dateline, ( $7^\circ \text{ S}-5^\circ \text{ N}$ ,  $160^\circ \text{ E}-180^\circ \text{ E}$ ) and in a more confined region compared with the corresponding one where negative  $DSR-A_{NE}$  values prevail during the ENSO warm phases. Moreover, the maximum  $DSR-A_{NE}$  values are observed west of the corresponding minimum  $DSR-A_{NE}$  values during the warm phases of ENSO. Within the Niño-3.4 region no significant DSR anomalies are observed during the cold ENSO phase.

The Niño-3.4 index is very often used to define the phase and strength of ENSO events. We calculated the correlation coefficient given by linear regression of the time-series of the monthly DSR anomaly, for the study period 1984–2004, in each  $2.5 \times 2.5^\circ$  grid-box and the Niño-3.4 index, and found values less than  $-0.5$  (anti-correlation) over

6713

the central tropical Pacific. Correlation coefficient values of about  $-0.8$  are observed west of the Niño-3.4 region and around the equator ( $7^\circ \text{ S}-5^\circ \text{ N}$ ,  $160^\circ \text{ E}-160^\circ \text{ W}$ ). Thus, in this region, the average DSR anomaly, is a very useful index to describe and study ENSO events and can be used to assess whether or not El Niño or La Niña conditions prevail.

The DSR in the western Pacific shows less variability between warm and cold ENSO events compared with the same parameter in the central and eastern tropical Pacific. We investigated the covariability between the time-series of the mean regional DSR anomaly in the western Pacific ( $10^\circ \text{ S}-5^\circ \text{ N}$ ,  $120-140^\circ \text{ E}$ ) and the Niño-3.4 index, and found a significant correlation (coefficient equal to 0.6). The DSR-A changes between  $+20 \text{ Wm}^{-2}$  and  $-20 \text{ Wm}^{-2}$  between warm and cold ENSO events, respectively.

We further investigated the covariability between the time-series of mean regional anomalies of DSR ( $DSR-A$ ) in the north subtropical region ( $7-15^\circ \text{ N}$ ,  $150-170^\circ \text{ E}$ ) and the Niño-3.4 index. The DSR-A in this region leads the corresponding Niño-3.4 index by about 7 months. Thus DSR measurements in this region will be very useful for the study of the time evolution of El Niño events.

*Acknowledgements.* The ISCCP-D2 data were obtained from the NASA Langley Research Center (LaRC) Atmospheric Sciences Data Center (ASDC). The NCEP/NCAR Global Reanalysis Project data were obtained from the National Oceanic and Atmospheric Administration (NOAA) Cooperative Institute for Research in Environmental Sciences (CIRES) Climate Diagnostics Center, Boulder, Colorado, USA. The GADS data were obtained from the Meteorological Institute of the University of Munich, Germany (<http://www.meteo.physik.uni-muenchen.de/strahlung/aerosol/aerosol.htm>).

## References

- Allan, R. P., Slingo, A., Ringer, and M. A.: Influence of dynamics on the changes in tropical cloud radiative forcing during the 1998 El Niño, *J. Climate*, 15, 1979–1986, 2002.  
Amador, J. A., Alfaro, E. J., Lizano, O. G., and Magan, V. O.: Atmospheric forcing of the eastern tropical Pacific: A review, *Prog. Oceanogr.*, 69, 101–142, 2006.

6714

- Bjerknes, J.: A possible response of the atmospheric Hadley circulation to equatorial anomalies of ocean temperature, *Tellus*, 18, 820–829, 1966.
- Bjerknes, J.: Atmospheric teleconnections from the equatorial Pacific, *Mon. Weather Rev.*, 97, 163–172, 1969.
- 5 Cane, M. A., Matthias, M., and Zebiak, S. E.: A study of self excited oscillations of the tropical ocean–atmosphere system. Part I: Linear analysis, *J. Atmos. Sci.*, 47, 1562–1577, 1990.
- Cess, R. D., Wang, P. H., and Wielicki, B. A.: Cloud structure anomalies over the tropical Pacific during the 1997/1998 El Niño, *Geophys. Res. Lett.*, 28, 4547–4550, 2001.
- Chou, S.-H., Chou, M.-D., Chan, P.-K., Lin, P.-H., and Wang, K.-H.: Tropical warm pool surface  
10 heat budgets and temperature: Contrasts between 1997/98 El Niño and 1998/99 La Niña, *J. Climate*, 17, 1845–1858, 2004.
- Curtis, S. and Adler, R. : ENSO indices based on patterns of satellite-derived precipitation, *J. Climate*, 13, 2786–2793, 2000.
- Dijkstra, H. A. : The ENSO phenomenon: theory and mechanisms, *Adv. Geosci.*, 6, 3–15, 2006,  
15 <http://www.adv-geosci.net/6/3/2006/>.
- Fedorov, A. V., Harper, S. L., Philander, S. G., Winter, B., and Wittenberg, A.: How predictable is El Niño?, *B. Am. Meteorol. Soc.*, 84, 911–919, 2003.
- Fotiadi, A., Hatzianastassiou, N., Matsoukas, C., Pavlakis, K. G., Drakakis, E., Hatzidimitriou, D., and Vardavas, I.: Analysis of the decrease in the tropical mean outgoing shortwave  
20 radiation at the top of atmosphere for the period 1984–2000, *Atmos. Chem. Phys.*, 5, 1721–1730, 2005,  
<http://www.atmos-chem-phys.net/5/1721/2005/>.
- Fotiadi, A., Hatzianastassiou, N., Stackhouse, P. W., Matsoukas, C., Drakakis, E., Pavlakis, K. G., Hatzidimitriou, D., and Vardavas, I.: Spatial and temporal distribution of long-term  
25 short-wave surface radiation over Greece, *Q. J. Roy. Meteor. Soc.*, 132, 2693–2718, 2006.
- Hanley, D. E., Bourassa, M. A., O'Brien, J. J., Smith, S. R., and Spade, E. R.: A quantitative evaluation of ENSO indices, *J. Climate*, 16, 1249–1258, 2003.
- Harrison, M. J., Rosati, A., Soden, B. J., Galanti, E., and Tziperman, E. :An evaluation of air-sea flux products for ENSO simulation and prediction, *Mon. Weather Rev.*, 130, 723–732,  
30 2002.
- Hatzianastassiou, N. and Vardavas, I.: Shortwave radiation budget of the Northern Hemisphere using International Satellite Cloud Climatology Project and NCEP/NCAR climatological data,

6715

- J. *Geophys. Res.*, 104, 24 401–24 421, 1999.
- Hatzianastassiou, N. and Vardavas, I.: Shortwave radiation budget of the Southern Hemisphere using ISCCP C2 and NCEP/NCAR climatological data, *J. Climate*, 14, 4319–4329, 2001.
- Hatzianastassiou, N., Fotiadi, A., Matsoukas, C., Drakakis, E., Pavlakis, K. G., Hatzidimitriou, D., and Vardavas, I.: Long-term global distribution of Earth's shortwave radiation budget at the top of atmosphere, *Atmos. Chem. Phys.*, 4, 1217–1235, 2004a,  
5 <http://www.atmos-chem-phys.net/4/1217/2004/>.
- Hatzianastassiou, N., Katsoulis, B., and Vardavas, I.: Global distribution of aerosol direct radiative forcing in the ultraviolet and visible arising under clear skies, *Tellus*, 56B, 51–71, 2004b.
- 10 Hatzianastassiou, N., Fotiadi, A., Matsoukas, C., Drakakis, E., Pavlakis, K. G., Hatzidimitriou, D., and Vardavas, I.: Global distribution of Earth's surface short-wave radiation budget, *Atmos. Chem. Phys.*, 5, 2847–2867, 2005,  
<http://www.atmos-chem-phys.net/5/2847/2005/>.
- Jin, F. F.: An equatorial ocean recharge paradigm for ENSO. Part I: Conceptual model, *J. Atmos. Sci.*, 54, 811–829, 1997a  
15
- Jin, F. F.: An equatorial ocean recharge paradigm for ENSO. Part II: A stripped-down coupled model, *J. Atmos. Sci.*, 54, 830–847, 1997b.
- Kistler, R., Kalnay, E., Collins, W., Saha, S., White, G., Woollen, J., Chelliah, M., Ebisuzaki, W., Kanamitsu, M., Kousky, V., van den Dool, H., Jenne, R., and Fiorino, M.: The NCEP-NCAR  
20 50-Year Reanalysis: Monthly Means CD ROM and Documentation, *B. Am. Meteorol. Soc.*, 82, 247–268, 2001.
- Koepke, P., Hess, M., Schult, I., and Shettle, E. P.: Global aerosol data set, Rep. No. 243, Max-Planck Institut fur Meteorologie, Hamburg, Germany, 44 pp., 1997.
- McCreary, J. P. and Anderson, D. L. T.: An overview of coupled ocean-atmosphere models of El Niño and the Southern Oscillation, *J. Geophys. Res.*, 96, 3125–3150, 1991.
- 25 McPhaden, M. J., Busalacchi, A. J., Cheney, R., et al.: The tropical ocean-global atmosphere observing system: A decade of progress, *J. Geophys. Res.*, 103, 14 169–14 240, 1998.
- Neelin, J. D., Battisti, D. S., Hirst, A. C., Jin, F. F., Wakata, Y., Yamagata, T., and Zebiak, S. E.: ENSO theory, *J. Geophys. Res.*, 103, 14 262–14 290, 1998.
- 30 Ohmura, A. and Gilgen, H.: Re-evaluation of the global energy balance. Interactions between global climate subsystems: The legacy of Hann, *Geophys. Monogr.*, No. 75, International Union of Geodesy and Geophysics, 93–110, 1993.
- Ohmura, A., Gilgen, H., Hegner, H., Mueller, G., Wild, M., Dutton, E. G., Forgan, B., Froehlich,

6716

- C., Philippona, R., Heimo, A., Koenig-Langlo, G., McArthur, B., Pinker, R., Whitlock, C. H., and Dehne, K.: Baseline Surface Radiation Network (BSRN/WCRP): New precision radiometry for climate research, *B. Am. Meteorol. Soc.*, 79, 2115–2136, 1998.
- 5 Pavlakis, K. G., Hatzidimitriou, D., Drakakis, E., Matsoukas, C., Fotiadi, A., Hatzianastassiou, N., and Vardavas, I.: ENSO surface longwave radiation forcing over the tropical Pacific, *Atmos. Chem. Phys.*, 7, 2013–2026, 2007, <http://www.atmos-chem-phys.net/7/2013/2007/>.
- Philander, S. G.: *El Niño, La Niña, and the Southern Oscillation*, Academic Press, San Diego, CA, 1–289, 1990.
- 10 Picaut, J., Masia, F., and du Penhoat, Y.: An advective–reflective conceptual model for the oscillatory nature of the ENSO, *Science*, 277, 663–666, 1997.
- Rossow, W. B. and Schiffer, R. A.: Advances in understanding clouds from ISCCP, *B. Am. Meteorol. Soc.*, 80, 2261–2288, 1999.
- Suarez, M. J. and Schopf, P. S.: A delayed action oscillator for ENSO, *J. Atmos. Sci.*, 45, 3283–3287, 1988.
- 15 Tian, B. and Ramanathan, V.: Role of tropical clouds in surface and atmospheric energy budget, *J. Climate*, 15, 296–305, 2002.
- Trenberth, K. E.: The definition of El Niño, *B. Am. Meteorol. Soc.*, 78, 2771–2777, 1997.
- Trenberth, K. E. and Caron, J. M.: The Southern Oscillation revisited: Sea level pressure, surface temperatures, and precipitation, *J. Climate*, 13, 4358–4365, 2000.
- 20 Trenberth, K. E. and Stepaniak, D. P.: Indices of El Niño evolution, *J. Climate*, 14, 1697–1701, 2001.
- Vardavas, I. and Carver, J. H.: Solar and terrestrial parameterizations for radiative convective models, *Planet. Space Sci.*, 32, 1307–1325, 1984.
- 25 Vardavas, I. M. and Taylor, F. W.: *Radiation and Climate*, International Series of Monographs on Physics, No. 138, Oxford University Press, Oxford, 2007.
- Wagner, T., Beirle, S., Grzegorski, M., Sanghavi, S., and Platt, U.: El Niño induced anomalies in global data sets of total column precipitable water and cloud cover derived from GOME on ERS-2, *J. Geophys. Res.*, 110, D15104, doi:10.1029/2005JD005972, 2005.
- 30 Wang, C., Weisberg, R. H., and Virmani, J. I.: Western Pacific interannual variability associated with the El Niño–Southern Oscillation, *J. Geophys. Res.*, 104, 5131–5149, 1999.
- Wang, C. and Weisberg, R. H.: The 1997–98 El Niño evolution relative to previous El Niño events, *J. Climate*, 13, 488–501, 2000.

6717

- Wang, C.: On the atmospheric responses to tropical Pacific heating during the mature phase of El Niño, *J. Atmos. Sci.*, 57, 3767–3781, 2000.
- Wang, C.: A unified oscillator model for the El Niño–Southern Oscillation, *J. Climate*, 14, 98–115, 2001.
- 5 Wang, C.: Atmospheric circulation cells associated with the El Niño–Southern Oscillation, *J. Climate*, 15, 399–419, 2002.
- Wang, C. and Picaut, J.: Understanding ENSO Physics: A review in Earth's Climate, in: *The Ocean-Atmosphere Interaction*, edited by: Wang, C., Xie, S.-P., and Carton, J. A., American Geophysical Union, 21–48, 2004.
- 10 Wang, C. and Fiedler, P. C.: ENSO variability and the eastern tropical Pacific: A review, *Prog. Oceanogr.*, 69, 239–266, 2006.
- Wolter, K. and Timlin, M. S.: Measuring the strength of ENSO events: How does 1997/98 rank?, *Weather*, 53, 315–324, 1998.

**Table 1.** Definition of symbols used to represent radiation parameters.

Symbol	Definition
DSR	Downward shortwave radiation at surface
$DSR_{EN}$ , $DSR_{LN}$ , $DSR_{NE}$	Mean DSR when El Niño, La Niña, or neutral conditions prevail, respectively
$DSR-A_{LN}$	El Niño DSR anomaly with respect to the mean DSR for the La Niña years equal to $DSR_{EN}-DSR_{LN}$
$DSR-A_{NE}$	El Niño or La Niña DSR anomaly with respect to the mean DSR for the neutral years equal to $DSR_{EN}-DSR_{NE}$ or $DSR_{LN}-DSR_{NE}$
$DSR-A$	DSR anomaly with respect to all years DSR

6719

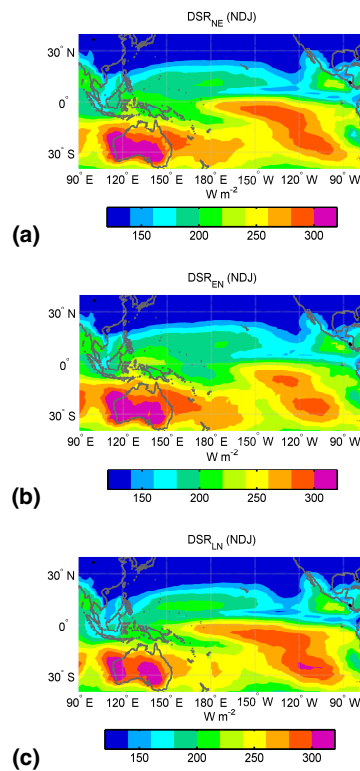


**Fig. 1.** The distribution of downward shortwave radiation at the surface (DSR), over the tropical and subtropical Pacific for the three month period November, December, January (NDJ); **(a)** eleven neutral years average, **(b)** average for five El Niño years, **(c)** average for five La Niña years.

6720

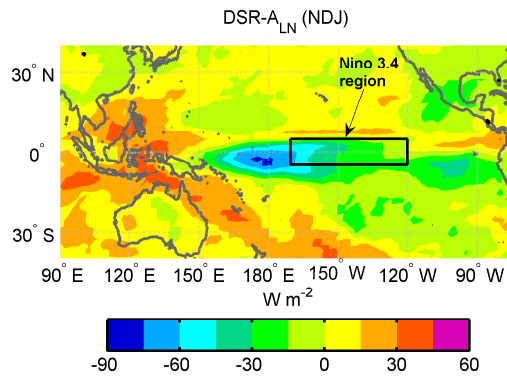


**Fig. 2.** Differences in the mean downward shortwave radiation at the surface (DSR), between the El Niño and La Niña years, over the tropical and subtropical Pacific for the period of November, December and January (NDJ).

6721

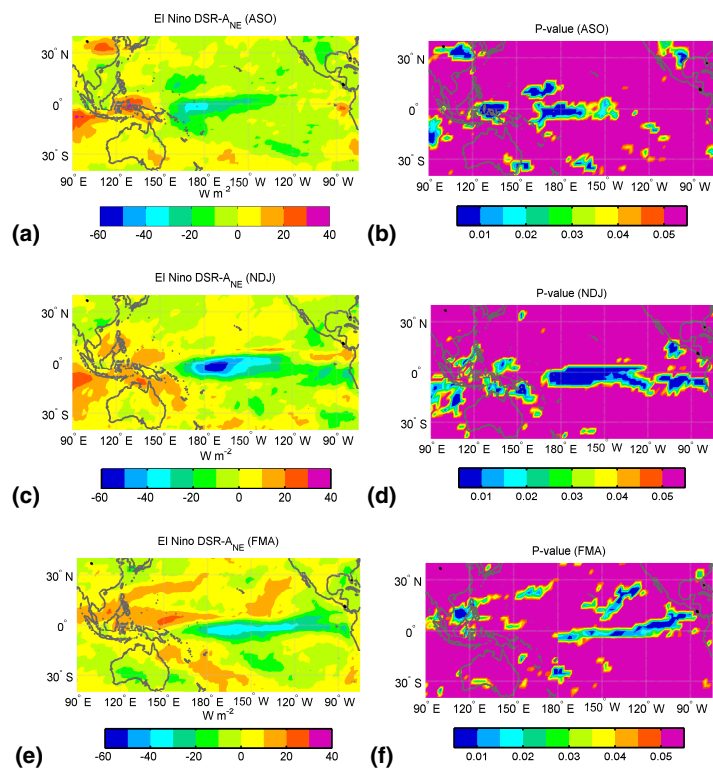


**Fig. 3.** Left: the distribution at  $2.5 \times 2.5$  spatial resolution of El Niño  $DSR-A_{NE}$  for ASO (top panel), NDJ (middle panel), and FMA (bottom panel). Right: the distribution of P-values from a Student's t-test.

6722

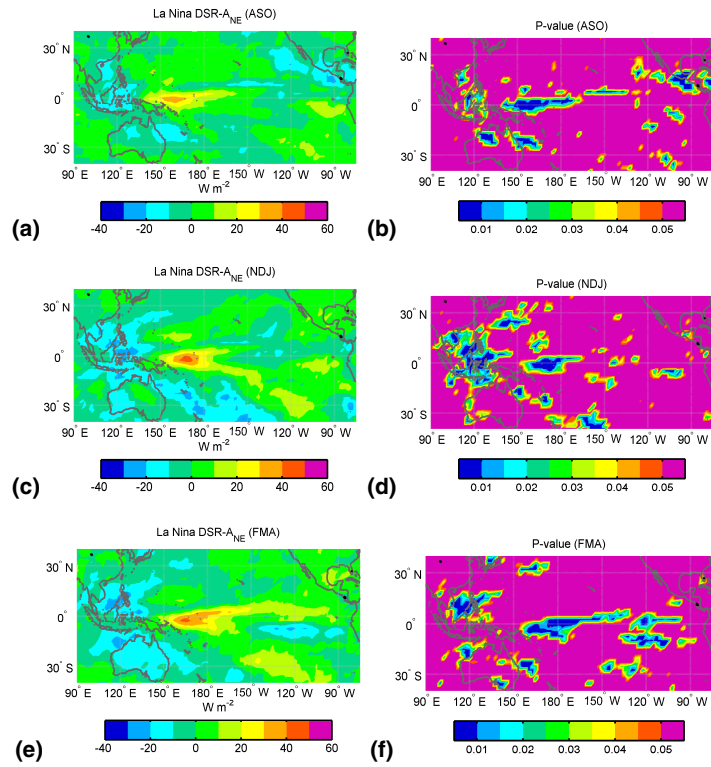


**Fig. 4.** Left: the distribution at  $2.5 \times 2.5$  spatial resolution of La Niña  $DSR-A_{NE}$  for ASO (top panel), NDJ (middle panel), and FMA (bottom panel). Right: the distribution of P-values from a Student's t-test.

6723

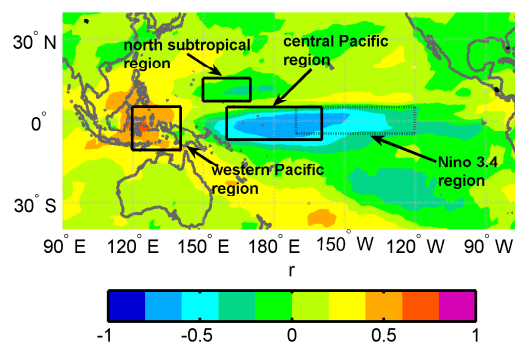


**Fig. 5.** Geographical distribution of correlation coefficient between DSR-A and the Niño-3.4 index.

6724

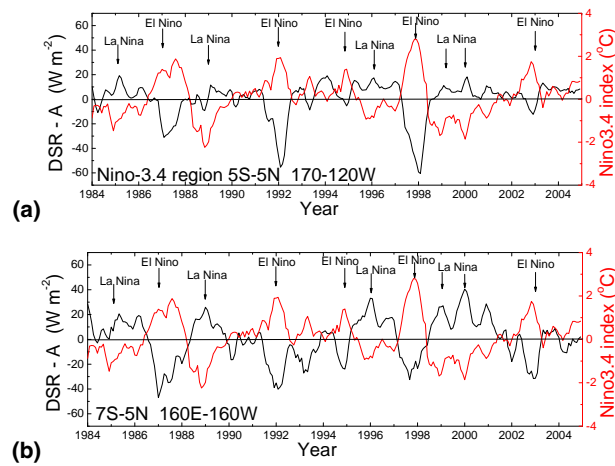


**Fig. 6.** Time-series of downward shortwave radiation anomaly (DSR-A) at the surface (defined with respect to the average monthly DSR for the whole study period 1984–2004) in the Niño-3.4 region **(a)**, and in the central Pacific region (7° S–5° N 160° E–160° W) **(b)**. Overlaid is the time-series of the Niño-3.4 index (red line).

6725

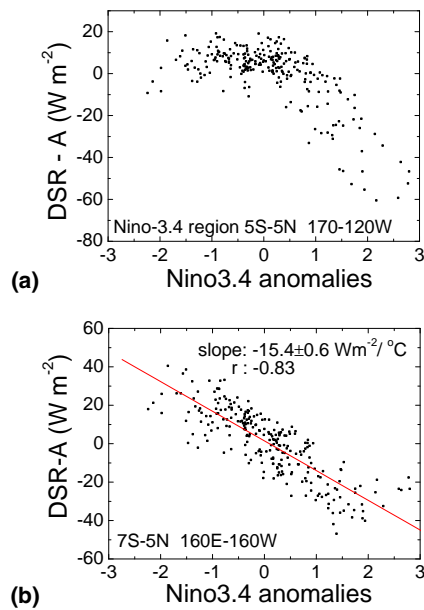


**Fig. 7.** Scatter plot between the Niño-3.4 index and the DSR-A in the: **(a)** Niño-3.4 region and **(b)** the central Pacific region (7° S–5° N 160° E–160° W).

6726

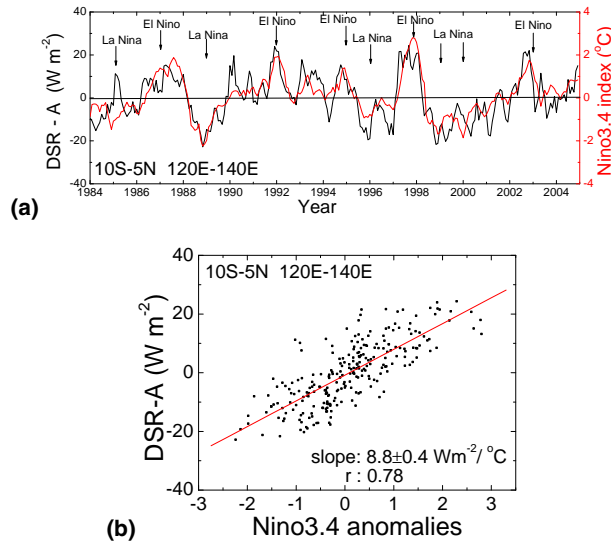


**Fig. 8.** (a) Time series of downward shortwave radiation anomaly (DSR-A) at the surface in the western Pacific region  $10^{\circ} S-5^{\circ} N$ ,  $120-140^{\circ} E$  (black line) compared with the time series of the Niño-3.4 index (red line). (b) Scatter plot between the DSR-A and the Niño-3.4 index in the western Pacific region.

6727

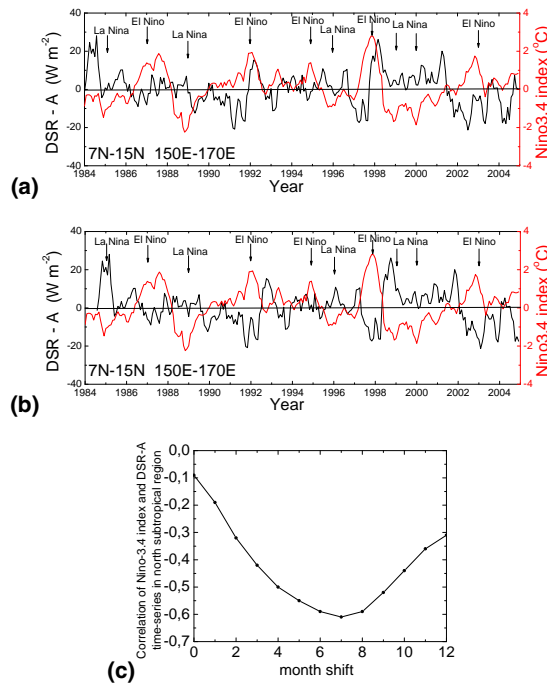


**Fig. 9.** (a) Time-series of downward shortwave radiation anomaly (DSR-A) at the surface (defined with respect to the average monthly DSR for the whole study period 1984–2004) in the north subtropical region ( $7-15^{\circ} N$   $150-170^{\circ} E$ ). Overlaid is the time-series of the Niño-3.4 index (red line). (b) The same as (a) but with the DSR-A time-series shifted by 7 months. (c) Correlation coefficient of the Niño-3.4 index and the DSR-A in the  $7^{\circ} N-15^{\circ} N$   $150-170^{\circ} E$  region as a function of the number of months shift of the DSR-A.

6728